The Astrophysical Journal Letters, 826:L21 (5pp), 2016 August 1 doi:10.3847/2041-8205/826/2/L21

LONG-LIVED SPIRAL STRUCTURE FOR GALAXIES WITH INTERMEDIATE-SIZE BULGES

Kanak Saha[1] and Bruce Elmegreen[2]
[1] Inter-University Centre for Astronomy and Astrophysics, Pune 411007, India; kanak@iucaa.in
[2] IBM Research Division, T. J. Watson Research Center, 1101 Kitchawan Road, Yorktown Heights, NY 10598, USA; bge@us.ibm.com
Received 2016 May 2; revised 2016 July 5; accepted 2016 July 7; published 2016 July 25

ABSTRACT

Spiral structure in disk galaxies is modeled with nine collisionless *N*-body simulations including live disks, halos, and bulges with a range of masses. Two of these simulations make long-lasting and strong two-arm spiral wave modes that last for ∼5 Gyr with constant pattern speed. These two had a light stellar disk and the largest values of the Toomre *Q* parameter in the inner region at the time the spirals formed, suggesting the presence of a *Q*-barrier to wave propagation resulting from the bulge. The relative bulge mass in these cases is about 10%. Models with weak two-arm spirals had pattern speeds that followed the radial dependence of the Inner Lindblad Resonance.

Key words: galaxies: bulges – galaxies: evolution – galaxies: halos – galaxies: kinematics and dynamics – galaxies: spiral – galaxies: structure

1. INTRODUCTION

Spiral structure in disk galaxies results from gravitationally amplified growth of density perturbations (Goldreich & Lynden-Bell 1965; Carlberg & Sellwood 1985; Toomre & Kalnajs 1991; Huber & Pfenniger 2002; see reviews in Athanassoula 1984; Bertin & Lin 1996) that range in scale from interstellar clouds (D'Onghia et al. 2013), to other spirals (Masset & Tagger 1997), to bars (Salo et al. 2010) and passing galaxies (Toomre & Toomre 1972; Salo & Laurikainen 2000). Simulated spiral arms are usually individually short-lived (Sellwood 2011; however, see Elmegreen & Thomasson 1993), although the presence of spiral structure in one form or another may be long-lived (Sellwood & Carlberg 2014).

Lindblad (1962, 1963) considered spirals "quasi-stationary" when he proposed they might result from synchronized epicyclic motions over a wide range of radii as viewed in a rotating coordinate system. This was a better model than material arms that would wrap up too quickly to explain the high fraction of disk galaxies with spirals. However, the correspondence noted by Lindblad was not perfect, and the proposed arms would still deform over time. Lin & Shu (1964) offered a solution to this problem by noting that arm self-gravity would perturb the epicycles in the right sense and cause them to lock into phase. Their solution was only a start, though, as Toomre (1969) pointed out that Lin–Shu waves also wrap up because their group velocity is inward.

The second part of this solution proposed that incoming waves refract or reflect in the central regions and move back out (Lin 1970; Mark 1976b). Then, they can amplify by disk gravity at corotation (CR) and send another trailing wave back in as well as a trailing wave out (Mark 1976a, 1976c). The result is a growing spiral wave mode, which is a standing wave with components moving in both directions (Mark 1977; Bertin et al. 1989a, 1989b). In the WASER type II mode discussed by Bertin (1983) and Lin & Bertin (1985) an inward-moving trailing spiral wave reflects off a high-*Q* barrier in the inner region, such as a bulge, and returns to CR as a weak leading wave. The leading wave then swings around into a stronger trailing wave in analogy to the swing amplifier proposed by Toomre (1981), and the trailing wave moves inward again. The outward moving trailing wave beyond CR extends to the outer Lindblad resonance where it resonates with the thermal motions of stars. For such a wave mode, the pattern speed is determined by the propagation condition for a wave to move in to the reflection radius and back out to CR in the time it takes the pattern to rotate to another arm (Bertin et al. 1989b).

Astronomical evidence for long-lived global modes is weak. Elmegreen & Elmegreen (1983) suggested that two-arm spirals live for at least ∼2 Gyr considering an observed increase in the fraction of such "grand designs" with galaxy group crossing rate and galaxy–galaxy collision rate. This duration corresponds to ∼5 rotations in the outer parts of a typical galaxy and is reasonably consistent with a spiral mode. Morphological evidence for spiral modes was suggested in Elmegreen et al. (1989) and Puerari et al. (2000) by the presence of symmetric spiral arm amplitude variations from interfering inward and outward moving waves (see also Bertin 1993). The arm variations observed for M81 were fit to the modal theory by Lowe et al. (1994). Further evidence for modes was shown in Elmegreen et al. (1992) by the presence of two-, three-, and four-arm symmetric spirals in 18 galaxies, with regular amplitude variations along the arms and arm endpoints at the appropriate Lindblad resonances. These latter two studies used computer-enhanced and symmetrized images to show features that are not obvious to the eye.

Modern simulations always have transient spiral features, even when they are wave modes (Sellwood 2011). This transience is partly because the modes adjust the radial distribution of stars and their velocity dispersions to change the basic state (Sellwood 2012), and they also trigger new modes that spring up at resonances of the old ones (Sygnet et al. 1988). Still, one wonders if a simulation with the right initial conditions can make a single, long-lasting wave mode in the sense discussed by Bertin et al. (1989b) and others. One essential component is a bulge that shields the inner Lindblad resonance (ILR) from incoming waves so they can reflect back to the amplification zone at CR. Otherwise, the ILR will absorb the wave (Lynden-Bell & Kalnajs 1972).

This Letter shows several examples of particle simulations that have a live disk, bulge, and halo and that appear to make single, long-lasting wave modes with constant pattern speeds. They have the strongest amplitude when the bulge is optimal for shielding the ILR. The models are in a sequence of increasing bulge mass, which also increases the strength of the

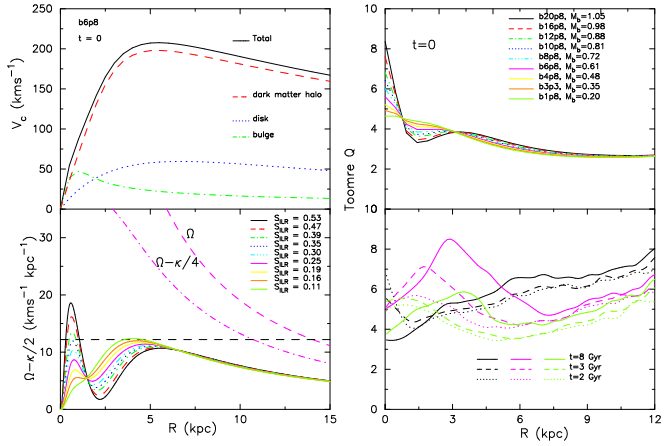

Figure 1. Initial setup and Q-bump during the growth of spiral arms. Top left panel: circular velocity curves. Bottom left panel: radial variation of Ω, $\Omega - \kappa/2$, $\Omega - \kappa/4$ for different model galaxies. $S_{\rm ILR}$ denotes the ILR strength defined in Section 2. Top right panel: initial Toomre Q-profiles for all the model galaxies. The bulge mass (M_b) is in units of $10^9\,M_\odot$. Bottom right panel: the Toomre Q-parameter vs. radius for models b20p8 (black), b6p8 (magenta), and b1p8 (green). Q for model b6p8 develops a peak in the inner region over time and grows strong spiral arms when the peak is largest (Figure 2). Model b1p8 has a smaller Q-peak later and grows a weak spiral later. Model b20p8 has no significant Q-peak and very weak arms throughout the simulation. Only the models with a Q-peak in the inner parts developed strong two-arm spirals, and they did this after the Q-peak appeared.

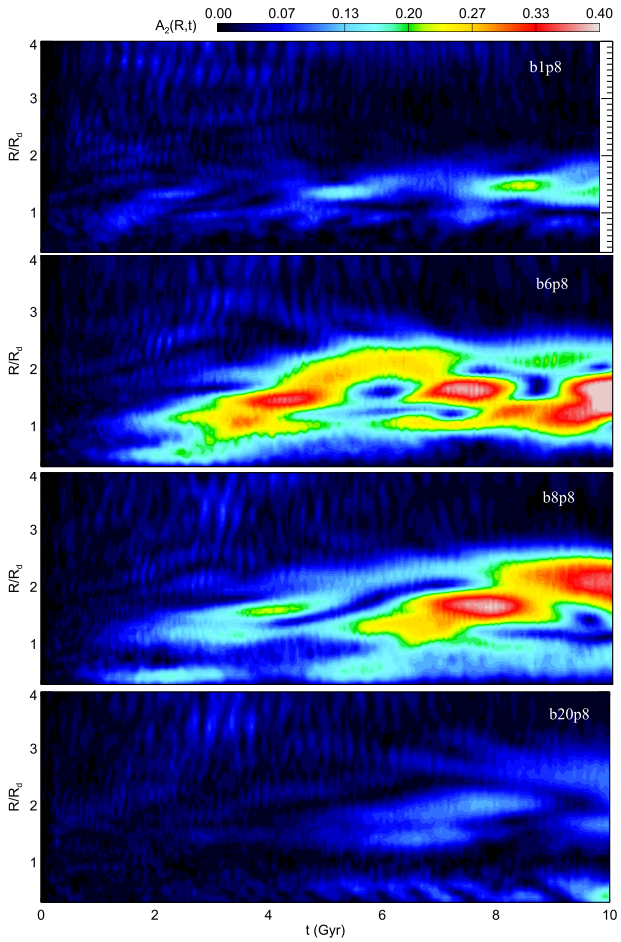

Figure 2. Spatio-temporal variation of the $m = 2$ Fourier amplitude in four models; $R_d = 3$ kpc. Model b20p8 has essentially no spiral structure.

ILR. For low-mass bulges, the ILR is weak but the bulges are also weak, and the spirals end up weak themselves. For high-mass bulges, the ILR absorption and bulge shielding are both strong but the ILR apparently wins again, making the waves weak. However, for intermediate-mass bulges, the conditions are optimal to make a strong and persistent two-arm wavemode, which circulates at constant pattern speed from ∼4 Gyr to ∼8 Gyr in the simulation. Eventually, the large arm amplitudes that result from this continuous growth can distort and destroy the spiral mode.

2. MODEL SETUP AND SIMULATION

We have constructed a set of nine initial equilibrium models of disk galaxies using the self-consistent method of Kuijken & Dubinski (1995). Each galaxy model consists of a stellar disk with an exponentially falling surface density; a flattened, cored dark-matter halo; and a classical bulge modeled with a King DF (for details, see Saha et al. 2012). All three components are live. In order to understand the role of the ILR, the disk and dark matter halo parameters are kept the same in all models, and only the total mass of the bulge (M_b) varies. This allows us to investigate the growth of spiral structure as a function of the bulge-to-total mass ratio (B/T). The initial variation of $\Omega - \kappa/2$ with radius is shown in the bottom left panel of Figure 1 for all models. The models are identified by an ILR strength, $S_{\rm ILR}$, which is defined to be the ratio of the peak value of $\Omega - \kappa/2$ in the inner parts to the rotation rate at 2 scale lengths, $\Omega(2R_{\rm d})$. The ILR for the $m = 2$ pattern occurs where the pattern speed equals $\Omega - \kappa/2$; the higher the bump at small $\Omega - \kappa/2$, the more likely there will be an ILR for the pattern speed chosen by the mass distribution.

The model number indicates the bulge central density (ρ_b), which is one of the parameters of a truncated King model, e.g., b10p8 corresponds to a $\rho_b = 10.8$ (internal units). Higher values of ρ_b correspond to higher bulge masses. Each model is scaled such that the scale length is $R_{\rm d} = 3$ kpc and the circular speed $V_c = 200$ km s^{-1} at $2R_{\rm d}$ (see Figure 1). The ratio of disk-to-halo mass $M_d/M_h = 0.07$ for all models—indicating a light stellar disk. For model b6p8, $M_d = 6.6 \times 10^9\,M_\odot$ and $M_h = 9.3 \times 10^{10}\,M_\odot$. The bulge mass varies from $0.2\times 10^9\,M_\odot$ for b1p8 to $1.0 \times 10^9\,M_\odot$ in b20p8; see Figure 1.

The initial stellar disk is relatively hot with Toomre $Q(R) \equiv \frac{\kappa\sigma_{\rm R}}{3.36G\Sigma}$ varying across the disk (top right panel of Figure 1). Q is relatively high because the stellar disk is comparatively low density. For example, model b6p8 has a central surface density of $\Sigma_0 = 117.4\,M_\odot$ pc^{-2}, which can easily be obtained from the total mass and length scale given above. This is about five times lower than that of Milky Way's stellar disk (Kuijken & Gilmore 1991). The radial velocity dispersion ($\sigma_{\rm R}$) also falls off exponentially with twice the scale length of the disk to keep the initial scale height constant at 300 pc for our stellar disk (Lewis & Freeman 1989; Kuijken & Dubinski 1995). The stars in the disk move under the epicyclic approximation (as per model construction), according to which the ratio of azimuthal to radial velocity dispersion follows the relation (Binney & Tremaine 1987):

$$\frac{\sigma_\varphi}{\sigma_{\rm R}} = \frac{\kappa}{2\Omega}. \quad (1)$$

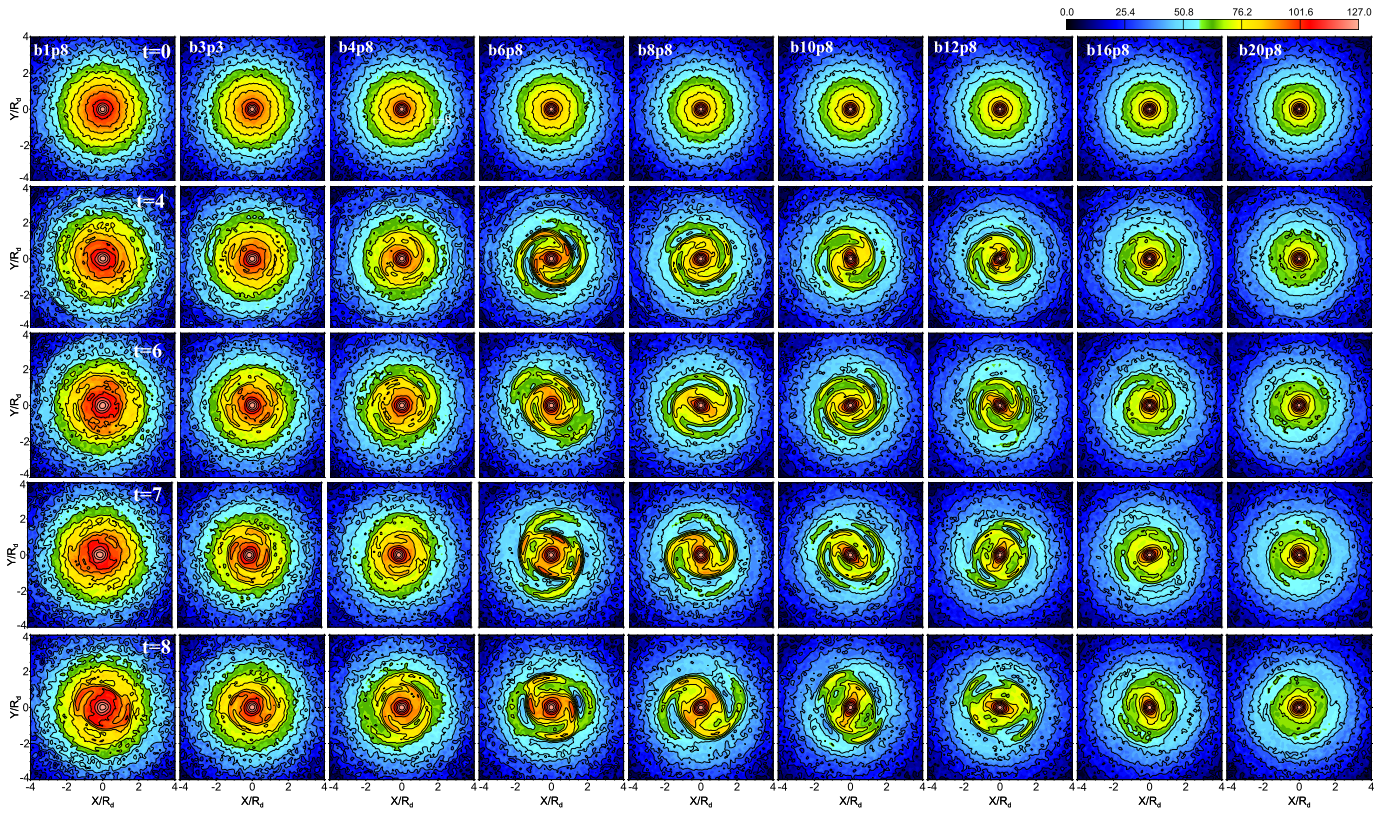

Figure 3. Face-on surface density maps for each model and their evolution. Time increases downward (in units of Gyr), and bulge mass increases from left to right. The labels for the models indicated at the top of each column correspond to bulge densities, as discussed in the text. The color scale at the top right corresponds to relative surface density. The leading spiral at $t = 7$ for b6p8 is the beginning of the outer ring visible at $t = 8$.

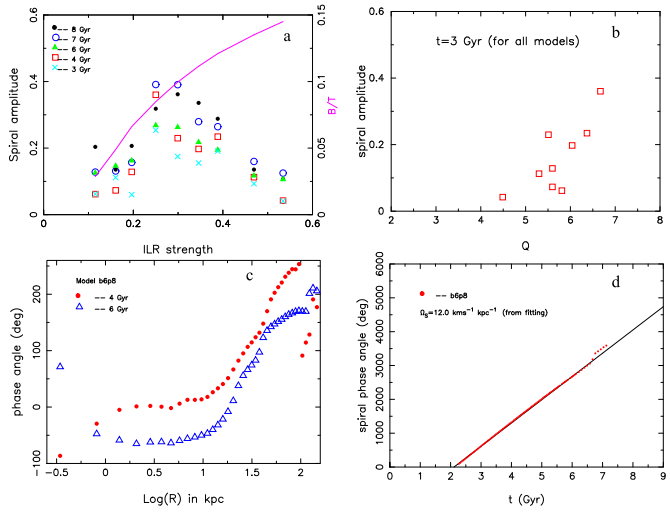

Figure 4. (a) Dependence of the Fourier $m = 2$ amplitude of the spiral pattern at the indicated times on ILR strength (defined in Section 2); pink solid line shows the dependence of B/T on the ILR strength. (b) Dependence on the peak value of Q computed at 3 Gyr. (c) Phase angle ($m = 2$) vs. natural log of radius in kpc. (d) The temporal variation of the phase angle at a given radius for the spiral mode run b6p8. The solid line is the linear fit to the phase angle vs. time; the slope is the pattern speed of 12.0 $\mathrm{kms^{-1}\,kpc^{-1}}$.

We have checked this for all the models at different times and found that the above relation holds pretty well. For example, for model b6p8, at $t = 2$ Gyr, at $2R_d$, $\kappa = 45.53$ km s^{-1} kpc^{-1} and $\Omega = 32.65$ km s^{-1} kpc^{-1} giving $\kappa/2\Omega = 0.697$. While $\sigma_R = 19.95$ km s^{-1} and $\sigma_\varphi = 14.02$ km s^{-1}, giving $\sigma_\varphi/\sigma_R = 0.7$ in good agreement. Note that $Q(R)$ varies with time as well, as the disk mass and stellar velocity dispersion change due to spiral forcing and heating (Jenkins & Binney 1990; Sellwood & Binney 2002; Saha et al. 2010; Roškar et al. 2012). $Q(R)$ is shown at three times during the simulation in the bottom right panel of Figure 1. The model with the highest peak in $Q(R)$, model b6p8 (magenta curve, $M_b = 0.61$), also has the strongest spiral structure at that time (see below).

We used a total of 2.2×10^6 particles to simulate each model galaxy of which 1.0×10^5 were in the classical bulge, 1.05×10^6 in the disk, and 1.05×10^6 in the dark matter halo. The time unit for model b6p8 is 45.3 Myr. The softening lengths for the disk, bulge, and halo were unequal and chosen so that the maximum force from particles of all species (bulge, disk, halo) is nearly the same (McMillan & Dehnen 2007). The simulations were performed with the Gadget code where forces between the particles were computed using a modified Barnes & Hut tree with a tolerance parameter $\theta_{tol} = 0.7$ (Springel et al. 2001).

3. GROWTH OF SPIRAL STRUCTURES

In order to characterize the growth of spiral structure in the simulated stellar disks, we compute the $m = 2$ Fourier component of the disk particle density and monitor its amplitude and phase variation across the disk as well as a function of time elapsed in the simulation. The development of spiral arms as a function of radius and time is shown in Figure 2, which plots the two-arm Fourier amplitude, $A_2(R, t)$,

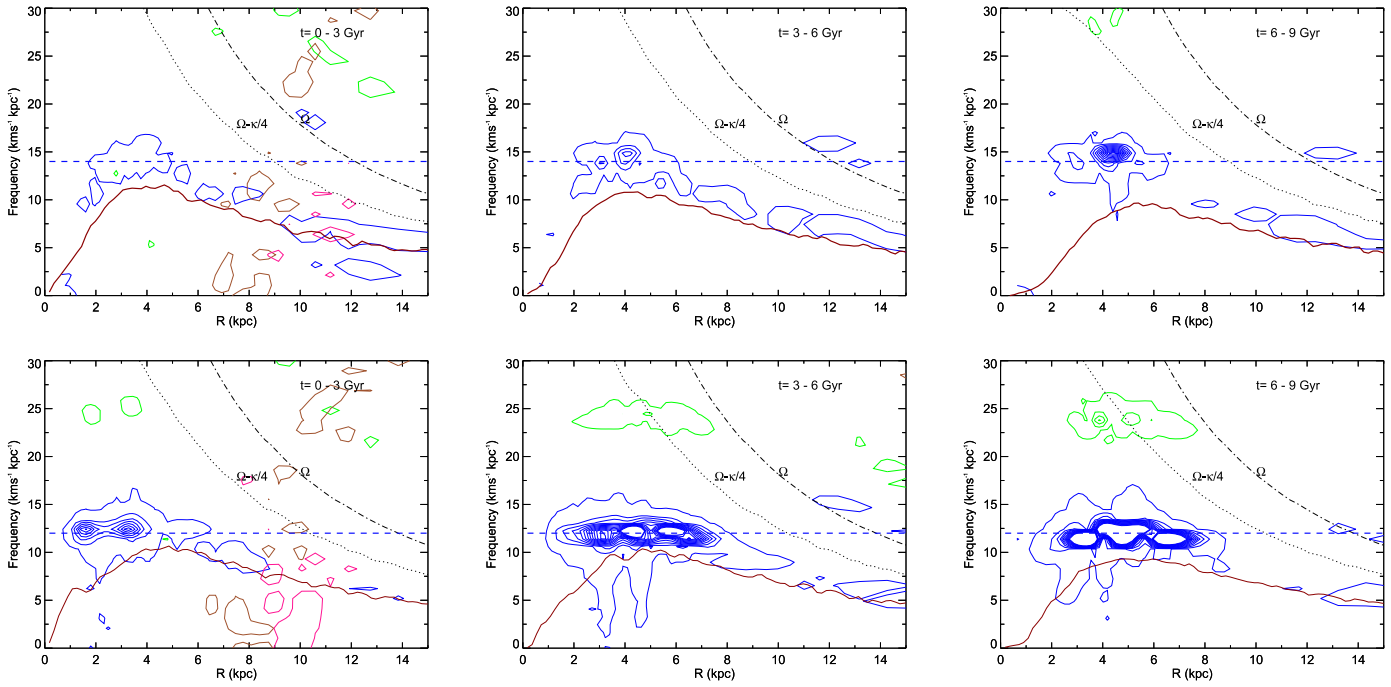

Figure 5. Basic dynamical frequencies and associated resonance locations at three different time intervals for models b1p8 (upper panels) and b6p8 (lower panels). Overplotted on this is the power spectrum for the $m = 2$ (in blue), $m = 4$ (green), $m = 6$ (brown), and $m = 8$ (pink) Fourier mode, computed at the indicated the time interval. The peak value of the power spectrum is 4×10^{-3}, while the outermost is at 2×10^{-5}. The strongest part of the spiral arms as shown by the contours ends in the inner region at the position of the Q-barrier, shown in the bottom right panel of Figure 1.

as a color scale for two strong (b6p8, b8p8) and two weak (b1p8, b20p8) spiral models. When there are $m = 2$ spirals, the amplitudes vary with time in pulses roughly separated by ∼3 Gyr at $R/R_{\rm d} \sim 1.5$–2, where the rotation time is ∼0.16 Gyr. The strongest two-arm spiral structure appears in model b6p8 hosting an intermediate bulge with $B/T = 0.085$; initially (up to about 4 Gyr), the spiral grows exponentially with a growth rate $\omega_I = 0.63$ km s^{-1} kpc^{-1}; after which the amplitude growth slows down with $\omega_I = 0.082$ km s^{-1} kpc^{-1}, showing signs of saturation. We also re-ran the model b6p8 with 6.15×10^6 particles (with 5 million in the halo) to check the effect of halo shot noise and found the primary results, e.g., pattern speed, spiral amplitude, unchanged; however, the growth of the spiral is delayed by about 1.4 Gyr with nearly the same growth rate $\omega_I = 0.66$ km s^{-1} kpc^{-1}.

Figure 2 also shows that at ∼3 Gyr, the spiral amplitude in model b6p8 faces a sudden growth. This growth is associated with a peak in the Toomre Q-profile (see Figure 1), which we interpret as a Q-barrier to the inward propagation of spiral arms. No other models had such a large Q-peak at that early time, but all of the models with large spiral amplitudes had a prominent Q-peak just before the spirals developed. Model b8p8 (with $B/T = 0.1$; Figure 2) grows strong two-arm spiral structure between 6 and 7 Gyr and has a strong Q-peak at that time. The same is true for model b1p8, although it formed only a weak spiral with no bar (Figure 2), after a weak inner Q-peak appeared (Figure 1) at ∼8 Gyr. The simultaneous occurrence of spiral structure and Q-peaks suggests some feedback effects in which an initially weak spiral changes the disk to produce a Q-peak, which, in turn, makes the spiral stronger. The model with a very high mass bulge, b20p8, evolved without growing either a Q-peak or a significant spiral.

Figure 3 shows the face-on surface density maps for all of the models at times of 0, 4, 6, 7, 8 Gyr. Model b1p8 on the left has the lowest mass bulge and evolves rather passively without making strong spirals until about 8 Gyr. As the bulge mass increases (moving to the right in the figure), the spiral structure becomes more prominent. As mentioned above, model b6p8 forms a strong, two-arm spiral at ∼3 Gyr and maintains that for the next ∼4 Gyr. Interestingly, just before 2 Gyr in this model, a weak and short (<1.5 kpc) bar-like structure that rotates with a different pattern speed, forms within the ILR. Images made from the disk particles show that this $m = 2$ feature resembles a nuclear bar; it disappears after ∼4 Gyr. Model b8p8 has an ILR strength slightly higher than that of b6p8 and the spiral structure in the initial phase is weaker, but it progressively becomes stronger and develops a bar-like feature eventually. b10p8 also develops spiral structure, but now there is a clear bar; the spiral dissolves gradually by 8 Gyr, and the bar grows stronger. Model b12p8 has an even stronger ILR and forms a comparatively weaker spiral structure associated with a bar. The other two models, b16p8 and b20p8, have massive bulges and higher ILR strengths but do not form any conspicuous spiral structure. It is interesting to note that both b1p8 and b20p8 did not grow a bar even after many tens of rotation times. Although b1p8 had no ILR, the disk was quite hot ($Q > 4$) and associated with a high value of the swing-amplification parameter (Binney & Tremaine 1987), $X = 14$ at $R = R_{\rm d}$, making the swing-amplification process ineffective.

Figures 4 (a) and (b) together suggest that the strongest spiral structure forms at intermediate ILR strengths and relative bulge masses, when the peak in $Q(R)$ is large. We interpret this Q-peak as a measure of the Q-barrier to the ILR. The radial variation of the phase angle at 4 and 6 Gyr suggest the presence of a bar-like structure that rotates with a pattern speed the same as the spiral in b6p8. This bar is also seen Figure 2 as a non-zero Fourier amplitude within $1R_d$ at early times, but it weakens

at later times (Figure 2), as may also be seen from the inner nearly circular density contours at late times in Figure 3.

3.1. Wavy Nature

It remains to be verified whether these spiral structures are density wave modes as proposed by Lin, Mark, Bertin, and others. Figure 4(d) shows the phase angle versus time for the $m = 2$ Fourier component of the spiral in run b6p8, which has the strongest arms at 4 Gyr. The phase angle was calculated in a radial range around the peak of the spiral amplitude, $R/R_{\rm d} = 1.2$. The phase increases regularly with time, indicating a constant pattern speed equal to the slope, $\Omega_{\rm p} = 12.0$ km s^{-1} kpc^{-1} from 2 to 7 Gyr. This pattern speed is shown by a dashed line in the lower panels of Figure 5, along with the other angular rates indicated. For each time interval, the $m = 2$ (blue), $m = 4$ (green), $m = 6$ (brown), and $m = 8$ (pink) Fourier power spectra for b6p8 were computed directly from the particle distributions (following Sellwood 1985; Masset & Tagger 1997) and overplotted as contours. The peak of the blue contours indicates a coherent spiral with a long-lasting pattern speed of ∼12.0 km s^{-1} kpc^{-1}, close to the peak of the ILR curve. The corotation resonance (CR) is where $\Omega_{\rm p} = \Omega(R)$ and lies at $R_{\rm cr} = 13.5$ kpc from the center. The strong spiral in model b8p8 also has a constant pattern speed, $\Omega_{\rm p} = 11.9$ km s^{-1} kpc^{-1}, which lasts for about 4.5 Gyr.

Higher-order waves have higher pattern speeds. The 4:1 resonance for the $m = 2$ pattern speed of model b6p8 is at 10.5 kpc ($3.5R_{\rm d}$) in Figure 5. A faint $m = 4$ spiral lies on that resonance at high frequency. There are more high-order waves at earlier times when the spirals are weak. The weak-spiral model b1p8 (Figure 5, upper panels) also has high-order waves at early times, along with weak $m = 2$ waves. These weak two-arm spirals follow the ILR with a pattern speed that varies with radius, reminiscent of Lindblad spirals caused by in-phase epicycles with weak gravity until about 8 Gyr, after which it rotates with a pattern speed $\Omega_p \simeq 14$ km s^{-1} kpc^{-1}. Generally, the strong spirals in our models stay within the 4:1 resonance, in compliance with K-band observations by Grosbol & Patsis (1998).

4. CONCLUSIONS

Two of our particle simulations with a live halo, bulge, and a light disk were found to generate spiral wave modes that grew slowly at first over a period of 1 to 2 Gyr and then quickly to a relatively large amplitude over the next 1 Gyr, after which they maintained a constant pattern speed for another 5 Gyr. These two simulations differed from the others, which did not make strong spiral arms, in the relative height of the maximum value of the Toomre Q-parameter in the inner region. This inner Q-peak results from the bulge. We interpret this result as evidence that wave reflection off a classical bulge can lead to the formation of a long-lasting spiral wave mode, as proposed by Bertin et al. (1989a).

The authors thanks the anonymous referee for several useful comments including the Fourier power spectrum (shown in Figure 5).

REFERENCES

Athanassoula, E. 1984, PhR, 114, 321
Bertin, G. 1983, in Proc. IAU Symp. 100, Internal Kinematics and Dynamics of Galaxies, ed. E. Athanassoula (Dordrecht: D. Reidel), 119
Bertin, G. 1993, PASP, 105, 640
Bertin, G., & Lin, C. C. 1996, Spiral Structure in Galaxies a Density Wave Theory (Cambridge, MA: MIT Press)
Bertin, G., Lin, C. C., Lowe, S. A., & Thurstans, R. P. 1989a, ApJ, 338, 78
Bertin, G., Lin, C. C., Lowe, S. A., & Thurstans, R. P. 1989b, ApJ, 338, 104
Binney, J., & Tremaine, S. 1987, Galactic Dynamics (Princeton, NJ: Princeton Univ. Press)
Carlberg, R. G., & Sellwood, J. A. 1985, ApJ, 292, 79
D'Onghia, E., Vogelsberger, M., & Hernquist, L. 2013, ApJ, 766, 34
Elmegreen, B. G., & Elmegreen, D. M. 1983, ApJ, 267, 31
Elmegreen, B. G., Elmegreen, D. M., & Montenegro, L. 1992, ApJS, 79, 37
Elmegreen, B. G., Seiden, P. E., & Elmegreen, D. M. 1989, ApJ, 343, 602
Elmegreen, B. G., & Thomasson, M. 1993, A&A, 272, 37
Goldreich, P., & Lynden-Bell, D. 1965, MNRAS, 130, 125
Grosbol, P. J., & Patsis, P. A. 1998, A&A, 336, 840
Huber, D., & Pfenniger, D. 2002, A&A, 386, 359
Jenkins, A., & Binney, J. 1990, MNRAS, 245, 305
Kuijken, K., & Dubinski, J. 1995, MNRAS, 277, 1341
Kuijken, K., & Gilmore, G. 1991, ApJL, 367, L9
Lewis, J. R., & Freeman, K. C. 1989, AJ, 97, 139
Lin, C. C. 1970, in Proc. IAU Symp. 38, The Spiral Structure of our Galaxy, ed. W. Becker & G. I. Kontopoulos (Dordrecht: Reidel), 377
Lin, C. C., & Bertin, G. 1985, in Proc. IAU Symp. 106, The Milky Way Galaxy, ed. H. van Woerden, R. J. Allen, & W. B. Burton (Dordrecht: D. Reidel), 513
Lin, C. C., & Shu, F. H. 1964, ApJ, 140, 646
Lindblad, B. 1962, in Proc. IAU Symp. 15, Problems of Extra-Galactic Research, ed. G. C. McVittie (New York: Macmillan), 146
Lindblad, B. 1963, StoAn, 22, 5
Lowe, S. A., Roberts, W. W., Yang, J., Bertin, G., & Lin, C. C. 1994, ApJ, 427, 184
Lynden-Bell, D., & Kalnajs, A. J. 1972, MNRAS, 157, 1
Mark, J. W.-K. 1976a, ApJ, 203, 81
Mark, J. W. K. 1976b, ApJ, 205, 363
Mark, J. W.-K. 1976c, ApJ, 206, 418
Mark, J. W.-K. 1977, ApJ, 212, 645
Masset, F., & Tagger, M. 1997, A&A, 322, 442
McMillan, P. J., & Dehnen, W. 2007, MNRAS, 378, 541
Puerari, I., Block, D. L., Elmegreen, B. G., Frogel, J. A., & Eskridge, P. B. 2000, A&A, 359, 932
Roškar, R., Debattista, V. P., Quinn, T. R., & Wadsley, J. 2012, MNRAS, 426, 2089
Saha, K., Martinez-Valpuesta, I., & Gerhard, O. 2012, MNRAS, 421, 333
Saha, K., Tseng, Y., & Taam, R. E. 2010, ApJ, 721, 1878
Salo, H., & Laurikainen, E. 2000, MNRAS, 319, 393
Salo, H., Laurikainen, E., Buta, R., & Knapen, J. H. 2010, ApJL, 715, L56
Sellwood, J. A. 1985, MNRAS, 217, 127
Sellwood, J. A. 2011, MNRAS, 410, 1637
Sellwood, J. A. 2012, ApJ, 751, 44
Sellwood, J. A., & Binney, J. J. 2002, MNRAS, 336, 785
Sellwood, J. A., & Carlberg, R. G. 2014, ApJ, 785, 137
Springel, V., Yoshida, N., & White, S. D. M. 2001, NewA, 6, 79
Sygnet, J. F., Tagger, M., Athanassoula, E., & Pellat, R. 1988, MNRAS, 232, 733
Toomre, A. 1969, ApJ, 158, 899
Toomre, A. 1981, in The Structure and Evolution of Normal Galaxies, ed. S. M. Fall & D. Lynden-Bell (Cambridge: Cambridge Univ. Press), 111
Toomre, A., & Kalnajs, A. J. 1991, in Dynamics of Disc Galaxies, ed. B. Sundelius (Göteborgs: Göteborgs University and Chalmers University of Technology), 341
Toomre, A., & Toomre, J. 1972, ApJ, 178, 623